HHS Public Access

Author manuscript

J Nat Prod. Author manuscript; available in PMC 2022 January 23.

Published in final edited form as:

J Nat Prod. 2021 July 23; 84(7): 1930–1940. doi:10.1021/acs.jnatprod.1c00192.

Himalaquinones A–G, Angucyclinone-Derived Metabolites Produced by the Himalayan Isolate *Streptomyces* sp. PU-MM59

Yongyong Zhang,
Department of Pharmacy, College of Life Sciences, China Jiliang University, Hangzhou 310018, People's Republic of China; Center for Pharmaceutical Research and Innovation and Department of Pharmaceutical Sciences, College of Pharmacy, University of Kentucky, Lexington, Kentucky 40536, United States;

Mohsin T. Cheema,
Center for Pharmaceutical Research and Innovation and Department of Pharmaceutical Sciences, College of Pharmacy, University of Kentucky, Lexington, Kentucky 40536, United States; Institute of Microbiology and Molecular Genetics (MMG), University of the Punjab, Lahore 54590, Pakistan

Larissa V. Ponomareva,
Center for Pharmaceutical Research and Innovation and Department of Pharmaceutical Sciences, College of Pharmacy, University of Kentucky, Lexington, Kentucky 40536, United States

Qing Ye,
Markey Cancer Center, Department of Pharmacology and Nutritional Sciences, College of Medicine, University of Kentucky, Lexington, Kentucky 40536, United States

Tao Liu,
Center for Pharmaceutical Research and Innovation and Department of Pharmaceutical Sciences, College of Pharmacy, University of Kentucky, Lexington, Kentucky 40536, United States; Department of Natural Products Chemistry, School of Pharmacy, China Medical University, Shenyang 110122, People's Republic of China

Imran Sajid,
Institute of Microbiology and Molecular Genetics (MMG), University of the Punjab, Lahore 54590, Pakistan

Jürgen Rohr,
Department of Pharmaceutical Sciences, College of Pharmacy, University of Kentucky, Lexington, Kentucky 40536, United States

Corresponding Authors: **Khaled A. Shaaban** – Center for Pharmaceutical Research and Innovation and Department of Pharmaceutical Sciences, College of Pharmacy, University of Kentucky, Lexington, Kentucky 40536, United States; khaled_shaaban@uky.edu; **Jon S. Thorson** – Center for Pharmaceutical Research and Innovation and Department of Pharmaceutical Sciences, College of Pharmacy, University of Kentucky, Lexington, Kentucky 40536, United States; jsthorson@uky.edu.

Supporting Information

The Supporting Information is available free of charge at https://pubs.acs.org/doi/10.1021/acs.jnatprod.1c00192.
Workup isolation scheme, biological activities, and full spectroscopic data (HPLC/UV, HPLC/MS, HRMS, and NMR) of compounds **1**–**7** (PDF)

Complete contact information is available at: https://pubs.acs.org/10.1021/acs.jnatprod.1c00192

The authors declare the following competing financial interest(s): J.S.T. is a co-founder of Centrose (Madison, WI).

Qing-Bai She,
Markey Cancer Center, Department of Pharmacology and Nutritional Sciences, College of Medicine, University of Kentucky, Lexington, Kentucky 40536, United States

S. Randal Voss,
Department of Neuroscience, Ambystoma Genetic Stock Center, and Spinal Cord and Brain Injury Research Center, University of Kentucky, Lexington, Kentucky 40536, United States

Jon S. Thorson,
Center for Pharmaceutical Research and Innovation and Department of Pharmaceutical Sciences, College of Pharmacy, University of Kentucky, Lexington, Kentucky 40536, United States;

Khaled A. Shaaban
Center for Pharmaceutical Research and Innovation and Department of Pharmaceutical Sciences, College of Pharmacy, University of Kentucky, Lexington, Kentucky 40536, United States;

Abstract

Himalaquinones A–G, seven new anthraquinone-derived metabolites, were obtained from the Himalayan-based *Streptomyces* sp. PU-MM59. The chemical structures of the new compounds were identified based on cumulative analyses of HRESIMS and NMR spectra. Himalaquinones A–F were determined to be unique anthraquinones that contained unusual C-4a 3-methylbut-3-enoic acid aromatic substitutions, while himalaquinone G was identified as a new 5,6-dihydrodiol-bearing angucyclinone. Comparative bioactivity assessment (antimicrobial, cancer cell line cytotoxicity, impact on 4E-BP1 phosphorylation, and effect on axolotl embryo tail regeneration) revealed cytotoxic landomycin and saquayamycin analogues to inhibit 4E-BP1p and inhibit regeneration. In contrast, himalaquinone G, while also cytotoxic and a regeneration inhibitor, did not affect 4E-BP1p status at the doses tested. As such, this work implicates a unique mechanism for himalaquinone G and possibly other 5,6-dihydrodiol-bearing angucyclinones.

Graphical Abstract

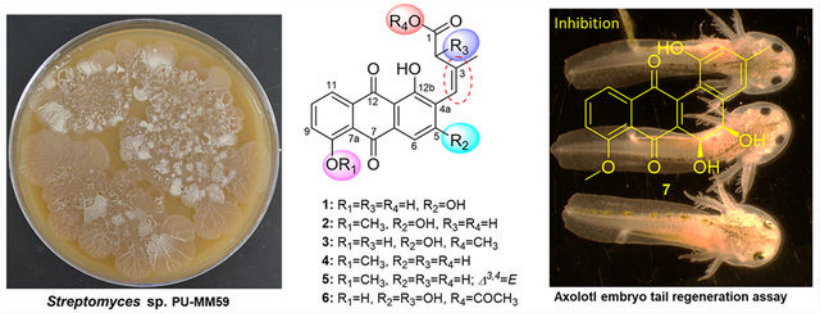

Angucyclines are ubiquitous aromatic polyketide metabolites signified by a benz[*a*]anthraquinone aglycone, variation in the A and B ring oxidation state, and differential glycosylation commonly observed on the A, B, and D rings (at the 3-, 8-, 9-, and/or 12b-positions).[1–18] These fused tetracyclic aromatic metabolites contribute to a

range of molecular mechanisms that primarily manifest in potent anticancer and antibacterial activities.[19–24] Thus, the discovery of novel angucycline natural products sets the stage for new bioactive probe development and provides access to unique genomic tools for biosynthetic and bioengineering efforts.[25–27] Within this context, we report the discovery of seven new microbial aromatic polyketides (himalaquinones A–G, **1**–**7**; Chart 1 and Supporting Information, Figure S3), produced by *Streptomyces* sp. PU-MM59 isolated from a Himalayan region of Pakistan. Six of these new metabolites [himalaquinones A–F (**1**–**6**)] were identified as classic anthraquinones bearing unusual C-4a 3-methylbut-3-enoic acid aromatic substitutions. Importantly, only three other such 3-methylbut-3-enoic acid-bearing anthraquinones have been reported, all of which are modified at the anthraquinone C-12b.[28] In addition, himalaquinone G (**7**) is a new 5,6-dihydrodiol-bearing angucyclinone, an angucycline subclass for which only three other members have been reported (PM070747, PD 116740, and TAN-1085; Supporting Information, Figure S1).[1,29–31] Herein, we describe the fermentation, isolation, and structure elucidation of himalaquinones A–G (**1**–**7**) and propose a biosynthetic pathway for these structurally unique metabolites based on well-established precedent. In addition, **1**–**7**, along with a diverse range of representative naturally occurring angucyclin(on)es (aquayamycin, rabelomycin, landomycins, saquayamycins, and urdamycin A) were evaluated for cancer cell line cytotoxicity, antimicrobial activity, inhibition of 4E-BP1 phosphorylation, and modulation of axolotl embryo development and tail regeneration.[32–37] These studies revealed angucyclinone **7** as an inhibitor of axolotl embryo tail regeneration and cancer cell line growth and suggest the antiproliferative mechanism of **7** may be unique to that of classical angucyclines. As such, this work may prompt further studies to elucidate the potentially unique fundamental mechanism of 5,6-dihydrodiol-bearing angucyclinones.

RESULTS AND DISCUSSION

Streptomyces sp. PU-MM59 was isolated from a soil sample collected 30 km east of Muzaffarabad City (Kashmir, Pakistan) as part of an ongoing effort to profile microbes and their metabolites from unique environments in Pakistan.[32,38–40] Metabolic profiling of more than 20 strains isolated from this soil sample implicated *Streptomyces* sp. PU-MM59 as capable of unique metabolite production based on an AntiBase 2017[41] database comparison. Scale-up fermentation (20 L) of *Streptomyces* sp. PU-MM59, followed by extraction, fractionation, and iterative chromatography (HP20 resin column chromatography, Sephadex LH-20 column chromatography, and semipreparative C_{18} HPLC), afforded seven pure metabolites (Supporting Information, Figure S3). On the basis of the cumulative MS and NMR spectral data analyses, these metabolites were identified and characterized as himalaquinones A (**1**, yield: 1.17 mg/L), B (**2**, yield: 0.12 mg/L), C (**3**, yield: 0.18 mg/L), D (**4**, yield: 0.24 mg/L), E (**5**, yield: 0.11 mg/L), F (**6**, yield: 0.38 mg/L), and G (**7**, yield: 0.20 mg/L).

The physicochemical properties of **1**–**7** are summarized in the Experimental Section. Compound **1** was obtained as a yellow-brown solid. The molecular formula of **1**, deduced as $C_{19}H_{14}O_7$ based on (+)-HRESIMS, indicated 13 degrees of unsaturation. The UV/vis spectrum of **1** displayed absorbance signatures common to anthraquinones.[42–45] The ^{13}C

NMR spectrum of **1** (Table 1 and Supporting Information, Figure S10) revealed 19 carbon resonances consistent with three carbonyl carbons, 14 sp^2 carbons, one methylene carbon, and one methyl carbon. Among these, the signals for two carbonyl resonances (δ_C 187.2 and 185.3) and 12 benzenoid carbons (rings B and D) were consistent with an anthraquinone core. The ^{1}H NMR of **1** (Table 2 and Supporting Information, Figure S9) included signals for four aromatic protons, one olefinic proton (δ_H 6.00, H-4), one methylene (δ_H 2.90, CH_2-2), one methyl (δ_H 1.99, 3-CH_3), and four hydroxy protons (Table 2). Among these, the presence of three *ortho*-coupled aromatic protons at δ_H 7.75 (1H, t, J = 8.0 Hz, H-10), 7.65 (1H, d, J = 7.5 Hz, H-11), and 7.30 (1H, d, J = 8.4 Hz, H-9) was consistent with a trisubstituted benzenoid moiety, further supported by the observation of COSY and NOESY cross-peaks for H-10/H-11 and H-9/H-10 and HMBC correlations (H-11 to C-9, C-7a, C-12; H-10 to C-8, C-11a; H-9 to C-11, C-7a) (Figure 1 and Supporting Information, Figures S11–S14). The annotation of the remaining aromatic proton at δ_H 7.24 (1H, s, H-6) was supported by HMBC correlations [H-6 to C-7, C-6a, C-4, C4a, C-12a]. Two chelated hydroxy proton signals were observed at δ_H 13.20 (12b-OH) and 12.38 (8-OH), consistent with the HMBC correlations [12b-OH with C-4a, C-12a, C-12b; 8-OH with C-7a, C-8, C-9]. The 3-methylbut-3-enoic acid substructure of **1** was deduced from the existence of one olefinic proton (δ_H 6.00, H-4), one methylene (δ_H 2.90, CH_2-2), and one methyl (δ_H 1.99, 3-CH_3), by the cumulative analysis of the molecular formula and by HSQC and HMBC correlations [H-4 with 3-$\underline{C}H_3$, C-2; 3-C$\underline{H}_3$ with C-2, C-3, C-4; and CH_2-2 with C-1, C-3, 3-$\underline{C}H_3$, C-4]. The HMBC correlations of H-4 to C-12b, C-4a, and C-4 served as key evidence for the C-4a aromatic substitution. The configuration of the double bond at C-3/C-4 was confirmed as *Z/cis*-configuration based on the observed NOE cross-peak between H-4 and 3-CH_3, consistent with H-4 and 3-CH_3 as adopting the same facial orientation (Figure 1). The remaining two hydroxy protons were assigned as 5-OH and CO$\underline{OH}$ (δ_H 11.80, 2H, br s). This was consistent with the observed downfield carbon shifts at C-5 (δ_C 162.8) and the carboxylic acid carbonyl (δ_C 172.0) (Figure 1 and Table 1). Based on this cumulative analysis, the structure of **1** was established as depicted in Figure 1. As a new natural product, **1** was named himalaquinone A to reflect the producing strain's point of origin.

Compounds **2** and **3** were isolated as yellow-brown solids. Both shared an identical molecular formula of $C_{20}H_{16}O_7$ established by (−)-HRESIMS. The ^{13}C NMR and ^{1}H NMR data of **2** and **3** (Tables 1 and 2) were similar to those of **1**, with the exception of ^{13}C (δ_C 56.4 and 51.3 for **2** and **3**, respectively) and ^{1}H (δ_H 3.94, 3H, s and δ_H 3.56, 3H, s for **2** and **3**, respectively) resonances consistent with an additional methoxy group (HSQC spectra, Supporting Information, Figures S21 and S30). Regiochemistry of **2** and **3** methylation was confirmed by the HMBC correlations (**2**, 8-OC$\underline{H}_3$ to C-8; **3**, OCH_3-13 to C-1). Similar to **1**, the *Z/cis*-configuration of the 3-methylbut-3-enoic acid double bond in **2** and **3** was established by NOESY (Figure 1). Cumulative analyses of 1D (^{1}H, ^{13}C) and 2D (HSQC, ^{1}H,^{1}H–COSY, HMBC, and NOESY) (Figure 1 and Tables 1 and 2) established the structures of **2** and **3** as depicted in Figure 1. Thus, the structures of **2** and **3** were established as new natural products and subsequently named as himalaquinones B and C, respectively.

Compounds **4** and **5** were obtained as yellow-brown solids and displayed UV–vis characteristics similar to metabolites **1**–**3**. Compounds **4** and **5** shared identical molecular

formulas of $C_{20}H_{16}O_6$ based on (+)-HRESIMS indicative of one oxygen less than **2** or **3**. Comparison of the ^{1}H NMR of **2** and **4** (Table 2) revealed **4** to lack the 5-OH hydroxy resonance of **2** (δ_H 11.80) and instead contain a new doublet proton signal at δ_H 7.72 (d, J = 7.9 Hz), consistent with the presence of ^{1}H–^{1}H COSY and NOE cross-peak H-5/H-6 for **4** (Figure 1; Supporting Information, Figures S38 and S41). All the remaining 2D NMR (^{1}H,^{1}H–COSY, HMBC, and NOESY) correlations are in full agreement with structure **4** (Figure 1). Based on the cumulative spectroscopic data, **4** and **5** differed solely via their C-3/C-4 double-bond configurations. Distinct from **1**–**4**, the *E/trans*-configuration in **5** was supported by an upfield chemical shift of 3-CH_3 (δ_C 18.4 in **5** compared to δ_C 24.5–23.9 in **1**-**4**; Table 1) as well as the observed NOE cross-peaks CH_2-2/H-4 and 3-CH_3/H-5 (Figure 1). Consistent with the cumulative 1D and 2D NMR data analysis, the structures of **4** and **5** were established as depicted in Figure 1 and named himalaquinones D and E, respectively.

Compound **6** was isolated as a yellow-brown solid with a molecular formula of $C_{21}H_{16}O_9$ based on (−)-HRESIMS. The ^{13}C/^{1}H/HSQC NMR of **6** (Tables 1 and 2; Supporting Information, Figures S54, S55, and S57) highlighted structural features of the C-4a aromatic substitution of **6** unique to those of **1**–**5**. Compared to **1**, the NMR spectra of **6** showed two additional carbons, including one carbonyl (δ_C 169.7) and one methyl signal (δ_C 20.4; δ_H 2.09, s). In addition, the methylene group (δ_H 2.90, s, H_2-2) of **1** was replaced with an oxygenated methine (δ_H 5.43, d, J = 0.9 Hz, H-2) in **6** along with the alterations of the chemical shifts at CH-4, C-3, 3-CH_3, CH-2, and C-1 positions (Tables 1 and 2). The planar structure of the side chain in compound **6** was confirmed through the HMBC correlations [H-4/C-2, C-3, 3-CH_3, C-4a, C-12b, C-5; 3-CH_3/C-2, C-3, C-4; H-2/C-1, C-3, 3-CH_3, C-4; CH_3-14/C-13] (Figure 1; Supporting Information, Figure S58). The C-3/C-4 double bond of **6** was consistent with the *Z/cis*-configuration [NOE cross-peak between H-4 and 3-CH_3] of **1**–**4**. In addition, the relative configuration of the C-2 stereocenter of compound **6** was established by NOESY, which highlighted H-2, 3-CH_3, and H-4 to adopt the same facial orientation (Figure 1; Supporting Information, Figure S59). Attempts to establish the absolute configuration at the C-2 stereocenter of **6** were unsuccessful. As a new natural product, **6** was subsequently designated as himalaquinone F.

In a similar manner, **7** was obtained as a yellow-green solid with a molecular formula of $C_{20}H_{16}O_6$ based on (+)-HRE-SIMS. Based on full 1D and 2D NMR analysis (Figure 1), the structure of **7** was deduced to be similar to PM070747[1] and PD 116740[29] (Supporting Information, Figure S1), with structural divergence via the C-3-substitution and 5,6-diol stereochemistry. Distinct from an ethyl group in PM070747 and a benzylic hydroxymethyl group in PD 116740, a methyl signal at δ_H 2.26 (3H, s, 3-CH_3) was observed in **7**, supported by HMBC correlations [3-CH_3/C-2, C-3, C-4; H-4/C-2, C-3, 3-CH_3, C-5, C-12b; H-2/3-CH_3, C-4, C-12b] (Figure 1 and Supporting Information, Figure S67). In addition, NOESY cross-peaks observed between H-4/3-CH_3 and 3-CH_3/H-2 were consistent with the methyl group at C-3 (Figure 1 and Supporting Information, Figure S68). A hydroxy group at C-1 was assigned based on the observed HMBC correlations from 1-OH (δ_H 9.64, s) to C-1, C-2, and C-12b. The presence of a 5,6-diol moiety was deduced by the observation of two coupled oxygenated methine protons at δ_H 4.36 (1H, d, J = 2.6 Hz, H-5) and 4.87 (1H, d, J = 2.5 Hz, H-6) as well as the HMBC correlations [H-6/C-4a, C-6a,

C-7; H-5/C-6, C-6a, C-4, C-12b]. Similar to **4** and **5**, three *ortho*-coupled protons at δ_H 7.77 (1H, t, J = 8.0 Hz, H-10), 7.51 (1H, overlap, H-9), and 7.49 (1H, overlap, H-11) for compound **7** were observed in the ^{1}H NMR/^{1}H–^{1}H COSY/NOESY spectra (Figure 1 and Table 2; Supporting Information, Figures S63, S65, and S68), indicating a trisubstituted benzene ring. This was further supported by the HMBC correlations [H-11/C-7a, C-12; H-10/C-11, C-9, C-11a; H-9/C-7a, C-11]. The C-8 methoxy was established based on the HMBC correlations from δ_H 3.93 (3H, s, 8-OCH$_3$) to C-8, as well as the NOESY cross-peak between H-9/8-OCH$_3$. The C-5/C-6 relative stereochemistry of **7** was established by NOESY (Figure 1 and Supporting Information, Figure S68), which highlighted H-4, H-5, and H-6 to adopt the same facial orientation (Figure 1; Supporting Information, Figure S68). Interestingly, an additional critical NOESY correlation between H-5/H-6 in **7** was observed that was not reported in PM070747[1] and PD 116740.[29] In addition, the smaller coupling constant (J = 2.5 Hz) in **7** compared to those of reported PM070747 and PD 116740 (J = 3 Hz) was also consistent with the H-5/H-6 *cis*-stereochemistry of **7**. Consistent with this, the determined optical rotation of **7** ($[\alpha]^{25}_D$ = −33.3, *c* 0.2, MeOH) was distinct from that reported for PM070747[1] (lit., $[\alpha]^{25}_D$ = +220, *c* 0.32, MeOH). As a new natural product, **7** was subsequently designated as himalaquinone G.

Given the structural novelty of the himalaquinones, Scheme 1 puts forth a putative biosynthetic pathway based on well-established angucyclinone precedent.[4,46–49] The earliest reported angucyclinone tetrangomycin likely serves as an early common intermediate.[50] Subsequent 8-*O*-methylation[46] affords 8-*O*-methyltetrangomycin, a putative point of biosynthetic divergence. A 3,4-elimination to 8-*O*-methyltetrangulol followed by dioxygenase- or sequential mono-oxygenase-catalyzed oxidation is postulated to provide **7**. Alternatively, Baeyer–Villiger monooxygenase-catalyzed lactone intermediate **A** formation is proposed to commit the pathway to metabolites **1**–**6**.[51–56] The hydrolysis of putative lactone **A** to fridamycin E[46,57–61] followed by *cis*- or *trans*-elimination and C-8 *O*-methylation would provide **4** and **5**. Alternatively, fridamycin E *cis*-elimination, C-8 *O*-methylation, and C-5 oxidation would give **1** and **2**. Metabolites **3** and **6** likely derive from **1** via methylation to ester **3** or side chain oxygenation and acetylation to anhydride **6**, respectively. C-8 or side chain *O*-glycosylation of fridamycin E could also give rise to fridamycin H[62] or gaudimycin D,[63] respectively.

Compounds **1**–**7** were initially evaluated in antimicrobial and cytotoxicity assays. Compounds **1**–**7** displayed weak anti-Gram-(+) (*Staphylococcus aureus*, *Micrococcus luteus*, and *Bacillus subtilis*) and anti-Gram-(−) (*Escherichia coli* and *Salmonella enterica*) activity at ≤133 μM. No detectable activity against mycobacteria (*Mycobacterium aurum*) or fungi (*Saccharomyces cerevisiae*) was observed at ≤133 μM. While anthraquinones **1**–**6** displayed little to no cancer cell line cytotoxicity at ≤80 μM concentration (Figure 2; Supporting Information, Figure S4), angucyclinone **7** displayed potent cytotoxicity against PC3 (prostate cancer cell line, IC$_{50}$ = 0.32 μM) and moderate cytotoxicity against A549 (non-small-cell lung cancer cell line, IC$_{50}$ = 1.88 μM) (Figure 2; Supporting Information, Table S1). In comparison, the structurally related analogues PM070747 and PD 116740 (Supporting Information, Figure S1) were nearly an order of magnitude less cytotoxic against comparable cancer cell lines.[1,29] Structurally similar cytotoxic natural products were

recently determined to function via inhibition of peroxiredoxin 1 (Prx1), leading to an increase of reactive oxygen species (ROS), subsequent inhibition of mTORC1-mediated 4E-BP1 phosphorylation (4E-BP1p), apoptosis induction, and tumor suppression.[34,37,64] Given the positive correlation between inhibition of 4E-BP1 phosphorylation and ROS-mediated cancer cell cytotoxicity in these studies, and the reported ability of angucyclines/angucyclinones to upregulate ROS and modulate mTORC1 function,[65–67] **7** and a representative set of related cytotoxic angucycline comparators were evaluated for their ability to inhibit 4E-BP1 phosphorylation. Specifically, this comparator test set included landomycins and saquayamycins that displayed IC_{50}s < 500 nM against A549 or PC3 (Figures 3 and 5; Supporting Information, Table S1).[2,3,5] As highlighted in Figure 3, a number of landomycins and saquayamycins were able to inhibit 4E-BP1p, while **7** lacked 4E-BP1p inhibitory activity at the doses tested. As a final measure of *in vivo* tolerance, antiproliferative efficacy, and potential impact on early development, **1**–**7** along with a diverse set of representative angucycline/angucyclinone comparators (compounds **8**–**31**) were also tested in an axolotl embryo tail regeneration assay (Figure 4; Supporting Information, Figure S5 and Table S1). Notably, nearly all angucyclines/angucyclinones tested in this *in vivo* assay were well-tolerated, and many inhibited tail regeneration at the doses evaluated (Figure 4).

CONCLUSIONS

In this study, we report the isolation, characterization, and bioactivities of six new anthraquinones and one unique angucyclinone from a Himalayan-based streptomyces. Himalaquinones A–F **(1**–**6**) were distinguished by their unusual anthraquinone C4a 3-methylbut-3-enoic acid side chains, while himalaquinone G (**7**) was identified as a rare 5,6-dihydrodiol angucycline analogue. Biosynthetically, **1**–**7** were postulated to diverge from a common tetrangomycin precursor following well-established anthraquinone and angucycline biosynthetic precedent. Bioactivity assessment revealed a putative mechanistic dichotomy among the angucyclines identified as potent cancer cell line cytotoxins (i.e., those displaying IC_{50}s ≤ 500 nM in either A549 and/or PC3) and inhibitors of *in vivo* tail regeneration. Specifically, this work revealed representative landomycin and saquayamycin analogues to inhibit 4E-BP1p, a strong correlation with ROS-mediated modulation of mTORC1 function[65,66] and cancer cell death. Consistent with this, representative landomycins were also previously reported to function via a ROS-mediated mechanism.[66,67] In contrast, the lack of **7** 4E-BP1p activity may implicate an alternative antiproliferative mechanism for **7** (and possibly PM070747 and PD 116740). As such, this study reinforces the concept that relatively minor structural modifications of classical natural product pharmacophores can dramatically alter mechanistic outcomes.

EXPERIMENTAL SECTION

General Experimental Procedures.

Optical rotation was measured on a Jasco DIP-370 digital polarimeter. UV spectra were recorded on a GE Ultraspec 8000 spectrophotometer (GE, Pittsburgh, PA, USA). NMR spectra were performed using a Varian (Palo Alto, CA, USA) Vnmr 400 (^{1}H, 400 MHz;

^{13}C, 100 MHz) spectrometer where δ-values were referenced to respective solvent signals [DMSO-d_6, δ_H 2.50 ppm, δ_C 39.51 ppm]. High-resolution electrospray ionization (HRESI) mass spectra were recorded on an AB SCIEX Triple TOF 5600 system. HPLC-MS analyses were accomplished with an Agilent 6120 Quadrupole MSD mass spectrometer (Agilent Technologies, Santa Clara, CA, USA) equipped with an Agilent 1200 Series Quaternary LC system and a Phenomenex NX-C_{18} column (250 × 4.6 mm, 5 μm; solvent A: H_2O/0.1% formic acid, solvent B: CH_3CN/0.1% formic acid; flow rate: 0.5 mL min^{-1}; 0–2 min, 5% B; 2–30 min, 5–100% B; 30–35 min, 100% B; 35–36 min, 100–5% B; 36–40 min, 5% B). Semipreparative HPLC was used on a Varian ProStar model 210 equipped with a photodiode array detector using a Supelco DiscoveryBio wide pore C_{18} column (21.2 × 250 mm, 10 μm). HPLC analyses were carried out in a Agilent 1260 system equipped with a photodiode array detector (PDA) and a Phenomenex C_{18} column (Phenomenex, Torrance, CA, USA; 250 × 4.6 mm, 5 μm; solvent A: H_2O/0.1% TFA, solvent B: CH_3CN; flow rate: 1.0 mL min^{-1}; 0–30 min, 5–100% B; 30–35 min, 100% B; 35–36 min, 100–5% B; 36–40 min, 5% B). All solvents used were of ACS grade and purchased from the Pharmco-AAPER (Brookfield, CT, USA). C_{18}-functionalized silica gel (40–63 μm) was purchased from Material Harvest Ltd. (Cambridge, UK). Amberlite XAD16N resin (20–60 mesh) and Diaion HP-20 resin (250–850 μm) were purchased from Sigma-Aldrich (St. Louis, MO; Bellefonte, PA, USA). Size exclusion chromatography was performed on Sephadex LH-20 (25–100 μm; GE Healthcare, Piscataway, NJ, USA). *Staphylococcus aureus*, *Bacillus subtilis, Mycobacterium aurum*, *Salmonella enterica*, and *Saccharomyces cerevisiae* strains and A549 and PC3 cells were obtained from ATCC (Manassas, VA, USA); *Micrococcus luteus* and *Escherichia coli* were obtained from NRRL (Peoria, IL, USA). All other reagents used were reagent grade and purchased from Sigma-Aldrich (St. Louis, MO, USA). Angucyclin(on)es **8**–**31** (Figure 5) used in this study were previously reported.[2,3,5,68]

Isolation and Identification of *Streptomyces* sp. PU-MM59.

The soil sample was collected near Pir Chinasi, 30 km east of Muzaffarabad City (Kashmir, Pakistan) at an elevation of 2900 m (coordinates: N 34°21′30″ and E 73°28′20″). Metabolic profiling and strain isolation followed previously reported protocols.[69–71] Strain identification, based on 16S rRNA sequencing following previously described protocols,[32,40] revealed 99% identity (BLAST search) with the 16S rRNA gene sequence of *Streptomyces* sp. strain D2Sl69. The 16S rRNA sequence of *Streptomyces* sp. PU-MM59 has been deposited in the NCBI nucleotide database with the accession number MH190054.

Fermentation, Extraction, Isolation, and Purification.

Streptomyces sp. PU-MM59 was cultivated on M2 agar plates [malt extract (10.0 g), glucose (4.0 g), yeast extract (4.0 g), $CaCO_3$ (2.0 g), and agar (18.0 g) dissolved in 1 L of H_2O (pH 7.2) and sterilized by autoclaving for 33 min at 121 °C] at 28 °C for 3 days. Small pieces of the agar with the fully grown strain were used to inoculate six 250 mL Erlenmeyer baffled flasks, each containing 50 mL of A-medium [glucose (10.0 g), yeast extract (5.0 g), soluble starch (20.0 g), peptone (5.0 g), NaCl (4.0 g), K_2HPO_4 (0.5 g), $MgSO_4 \cdot 7H_2O$ (0.5), and calcium carbonate (2 g) dissolved in 1 L of H_2O (pH 7.0) and sterilized by autoclaving for 33 min at 121 °C], and the culture was grown at 28 °C with shaking (210 rpm) for 3 days. An aliquot of seed culture (1 mL) was used to inoculate 200 250 mL

baffled flasks each containing 100 mL of A-medium. Fermentation was continued at 28 °C with 210 rpm agitation for 10 days. All 200 culture flasks were combined to obtain 20 L of yellowish-brown culture broth, which was subsequently centrifuged (5000 rpm, 20 min). The supernatant was extracted by mixing with XAD-16 (4%) resin overnight, followed by filtration. The resin was washed with water (2000 mL) and then extracted with MeOH (3 L). The methanolic extract was subsequently evaporated *in vacuo* to yield 19.6 g of yellowish-brown extract. The biomass (mycelium) was extracted with MeOH (5 × 800 mL) and then evaporated *in vacuo* to afford 33.6 g of yellowish-brown extract. After being analyzed with HPLC and TLC, both extracts showed an identical set of metabolites. Thus, the extracts were combined to get a total 53.2 g of crude extract for further separation.

As highlighted in Figure S3 (see Supporting Information), the combined extract (53.2 g) was subjected to an HP-20 resin column (column 6 × 26 cm) and eluted with a gradient of aqueous MeOH (0%, 20%, 40%, 60%, 80%, 100%; each 2.0 L) to afford five fractions, A–E (excluding the 0% MeOH fraction, which was discarded, as the HPLC profile matched that of the culture broth). The target compounds were detected in fractions D (1.26 g) and E (1.17 g), and both fractions were combined (2.43 g) based on their similarity in HPLC and TLC analyses. The combined fractions D and E (2.43 g) was subjected to a Sephadex LH-20 column (MeOH, 3 × 80 cm) to afford six subfractions, D1–D6. Subfraction D3 was separated by a Sephadex LH-20 column (MeOH, 2 × 40 cm) again to yield subfractions D3A–D3D. Further purification of D3A using semipreparative HPLC (mobile phase: 23% aqueous CH_3CN, flow rate: 8 mL min^{-1}, wavelength: 320 nm) afforded **7** (4.0 mg). Subfraction D5 was subjected to a reverse-phase C_{18} column (3 × 20 cm) and isolated with a gradient of aqueous MeOH (50–100%) to obtain subfractions D5A–D5G. Further purification of subfractions D5B and D5C by semipreparative HPLC (mobile phase: 35% aqueous CH_3CN, flow rate: 8 mL min^{-1}, wavelength: 280 nm) afforded **5** (2.2 mg) and **2** (2.3 mg), respectively. Subfractions D5E and D5F were combined due to their similar HPLC profiles and further resolved using semipreparative HPLC (mobile phase: 45% aqueous CH_3CN, flow rate: 8 mL min^{-1}, wavelength: 320 nm) to afford **4** (4.7 mg). In a similar manner, subfraction D6 was subjected to a reverse-phase C_{18} column (3 × 20 cm) with a gradient of aqueous MeOH (50–100%) to give subfractions D6A–D6H. Subfractions D6D, D6F, and D6H were further subjected to semipreparative HPLC purification (mobile phase: 65% aqueous MeOH for subfraction D6D; 40% aqueous CH_3CN for subfraction D6F; 48% aqueous CH_3CN for subfraction D6H, flow rate: 8 mL min^{-1}, wavelength: 320 nm) to yield **6** (7.6 mg), **1** (23.3 mg), and **3** (3.5 mg) in pure forms, respectively.

Himalaquinone A (1): yellow-brown solid; UV/vis (MeOH) λ_{max} (log ε) 214 (3.82), 237 (3.80), 289 (4.06), 431 (3.74) nm; ^{1}H NMR (DMSO-d_6, 400 MHz) and ^{13}C NMR (DMSO-d_6, 100 MHz), see Tables 1 and 2; (+)-ESIMS m/z 355 $[M + H]^+$, 377 $[M + Na]^+$; (−)-ESIMS m/z 353 $[M - H]^-$; (+)-HRESIMS m/z 355.0814 $[M + H]^+$ (calcd for $C_{19}H_{15}O_7$, 355.0812).

Himalaquinone B (2): yellow-brown solid; UV/vis (MeOH) λ_{max} (log ε) 223 (3.51), 241 (3.23), 286 (3.65), 418 (3.26) nm; ^{1}H NMR (DMSO-d_6, 400 MHz) and ^{13}C NMR (DMSO-d_6, 100 MHz), see Tables 1 and 2; (+)-ESIMS m/z 369 $[M + H]^+$, 391 $[M + Na]^+$,

759 [2 M + Na]$^+$; (−)-ESIMS *m*/*z* 367 [M − H]$^-$; (−)-HRESIMS *m*/*z* 367.0813 [M − H]$^-$ (calcd for $C_{20}H_{15}O_7$, 367.0823).

Himalaquinone C (3): yellow-brown solid; UV/vis (MeOH) λ_{max} (log ε) 220 (3.00), 237 (3.20), 287 (3.67), 431 (3.32) nm; ^{1}H NMR (DMSO-d_6, 400 MHz) and ^{13}C NMR (DMSO-d_6, 100 MHz), see Tables 1 and 2; (+)-ESIMS *m*/*z* 369 [M + H]$^+$, 391 [M + Na]$^+$; (−)-ESIMS *m*/*z* 367 [M − H]$^-$; (−)-HRESIMS *m*/*z* 367.0815 [M − H]$^-$ (calcd for $C_{20}H_{15}O_7$, 367.0823).

Himalaquinone D (4): yellow-brown solid; UV/vis (MeOH) λ_{max} (log ε) 225 (3.41), 271 (3.72), 415 (3.44) nm; ^{1}H NMR (DMSO-d_6, 400 MHz) and ^{13}C NMR (DMSO-d_6, 100 MHz), see Tables 1 and 2; (+)-ESIMS *m*/*z* 353 [M + H]$^+$, 375 [M + Na]$^+$, 727 [2 M + Na]$^+$; (−)-ESIMS *m*/*z* 351 [M − H]$^-$; (+)-HRESIMS *m*/*z* 353.1020 [M + H]$^+$ (calcd for $C_{20}H_{17}O_6$, 353.1020).

Himalaquinone E (5): yellow-brown solid; UV/vis (MeOH) λ_{max} (log ε) 218 (3.60), 242 (3.50), 273 (3.83), 428 (3.54) nm; ^{1}H NMR (DMSO-d_6, 400 MHz) and ^{13}C NMR (DMSO-d_6, 100 MHz), see Tables 1 and 2; (+)-ESIMS *m*/*z* 353 [M + H]$^+$, 375 [M + Na]$^+$, 727 [2 M + Na]$^+$; (+)-HRESIMS *m*/*z* 353.1023 [M + H]$^+$ (calcd for $C_{20}H_{17}O_6$, 353.1020).

Himalaquinone F (6): yellow-brown solid; $[\alpha]^{25}_D$ = +10.5 (*c* 0.4, MeOH); UV/vis (MeOH) λ_{max} (log ε) 220 (3.37), 243 (3.56), 288 (4.03), 430 (3.71) nm; ^{1}H NMR (DMSO-d_6, 400 MHz) and ^{13}C NMR (DMSO-d_6, 100 MHz), see Tables 1 and 2; (+)-ESIMS *m*/*z* 413 [M + H]$^+$, 435 [M + Na]$^+$, 847 [2 M + Na]$^+$; (−)-ESIMS *m*/*z* 411 [M − H]$^-$; (−)-HRESIMS *m*/*z* 411.0711 [M − H]$^-$ (calcd for $C_{21}H_{15}O_9$, 411.0722).

Himalaquinone G (7): yellow-green solid; $[\alpha]^{25}_D$ = −33.3 (*c* 0.2, MeOH); UV/vis (MeOH) λ_{max} (log ε) 215 (3.63), 243 (3.47), 274 (3.70), 381 (3.40) nm; ^{1}H NMR (DMSO-d_6, 400 MHz) and ^{13}C NMR (DMSO-d_6, 100 MHz), see Tables 1 and 2; (+)-ESIMS *m*/*z* 353 [M + H]$^+$, 375 [M + Na]$^+$, 727 [2 M + Na]$^+$; (−)-ESIMS *m*/*z* 351 [M − H]$^-$; (+)-HRESIMS *m*/*z* 353.1022 [M + H]$^+$ (calcd for $C_{20}H_{17}O_6$, 353.1020).

Antibacterial, Antifungal, and Cancer Cell Line Viability Assays.

Antibacterial (*Staphylococcus aureus* ATCC 6538, *Micrococcus luteus* NRRL B-287, *Bacillus subtilis* ATCC 6633, *Mycobacterium aurum* ATCC 23366, *Escherichia coli* NRRL B-3708, *Salmonella enterica* ATCC 10708), antifungal (*Saccharomyces cerevisiae* ATCC 204508), and mammalian cell line cytotoxicity [A549 (non-small-cell lung) and PC3 (prostate) human cancer cell lines] assays were accomplished in triplicate following our previously reported protocols.[70–72] Positive controls for antibacterial and antifungal assays included kanamycin and ampicillin (*S. aureus*, *M. luteus*, *S. enterica*, and *E. coli*) and amphotericin B (*S. cerevisiae*). Actinomycin D (A549 and PC3) was used as the positive control for cancer cell line viability assays (Figure 2 and Supporting Information, Figure S4).

Axolotl Embryo Tail Regeneration Assay.

The axolotl embryo tail regeneration assay was conducted following our previously reported protocols.[33–35] Briefly, stage 42 embryos were manually hatched, administered benzocaine anesthesia (0.2 g in 5 mL EtOH/L water), and photographed. Embryos were subsequently administered 2 mm tail amputations and then reared (in the absence or presence of test agent) at 18–19 °C in 12-well microtiter plates containing 2.0 mL of artificial pond water (43.25 g NaCl, 0.625 g KCl, 1.25 g $MgSO_4$, 2.5 g $NaHCO_3$, and 1.25 g $CaCl_2$ per 50 L charcoal filtered municipal water). Assays were conducted for 7 days postamputation (DPA). Images of anesthetized embryos at 0 and 7 DPA were captured using an Olympus microscope with a 0.5× objective lens and DP400 camera. All chemicals were dissolved in DMSO and diluted to 0.1% final DMSO concentration. Axolotls (RRID:AGSC_100E) were obtained from the Ambystoma Genetic Stock Center (RRID:SCR_006372). Vehicle (DMSO) was used as the negative control, and the Hsp90 inhibitor geldanamycin was used as a positive control.

Western Blot Analysis.

Western blot analysis was performed as previously described.[34,64] Specifically, after treatment with test agent, cells were lysed in NP-40 lysis buffer (50 mM Tris-HCl, pH 7.5, 150 mM NaCl, 1 mM EDTA, 1% NP-40, 10% glycerol, protease and phosphatase inhibitor cocktail). Equal amounts of lysate were subsequently resolved by SDS-PAGE, transferred to PVDF membranes, immunoblotted with specific primary and secondary antibodies, and detected using chemiluminescence (GE Healthcare, Chicago, IL, USA). Antibodies for phospho-4E-BP1 (Thr37/46) (#2855), phospho-4E-BP1 (Ser65) (#13443), and phospho-4E-BP1 (Thr70) (#13396) were purchased from Cell Signaling Technology (Danvers, MA, USA).

Supplementary Material

Refer to Web version on PubMed Central for supplementary material.

ACKNOWLEDGMENTS

This work was supported by National Institutes of Health grants R24 OD21479 (S.R.V., J.S.T.), R01 CA203257 (Q.B.S., J.S.T.), R01 CA175105 (Q.B.S.), R01 GM115261 (J.S.T.), the Center of Biomedical Research Excellence (COBRE) in Pharmaceutical Research and Innovation (CPRI, NIH P20 GM130456), the University of Kentucky College of Pharmacy, the University of Kentucky Markey Cancer Center, and the National Center for Advancing Translational Sciences (UL1TR000117 and UL1TR001998). This work was also supported by a Higher Education Commission (HEC) Pakistan grant (HEC-NRPU Project 2121). We thank the College of Pharmacy NMR Center (University of Kentucky) for NMR support.

REFERENCES

(1). Pérez M; Schleissner C; Rodríguez P; Zúñiga P; Benedit G; Sánchez-Sancho F; de la Calle F J. Antibiot 2009, 62, 167–169.

(2). Shaaban KA; Stamatkin C; Damodaran C; Rohr J J. Antibiot 2011, 64, 141–150.

(3). Shaaban KA; Srinivasan S; Kumar R; Damodaran C; Rohr J J. Nat. Prod 2011, 74, 2–11. [PubMed: 21188999]

(4). Kharel MK; Pahari P; Shepherd MD; Tibrewal N; Nybo SE; Shaaban KA; Rohr J Nat. Prod. Rep 2012, 29, 264–325. [PubMed: 22186970]

(5). Shaaban KA; Ahmed TA; Leggas M; Rohr J J. Nat. Prod 2012, 75, 1383–1392. [PubMed: 22758660]

(6). Baranczak A; Sulikowski GA Tetrahedron Lett 2012, 53, 1345–1346. [PubMed: 22383859]

(7). Sharif EU; O'Doherty GA Eur. J. Org. Chem 2012, 2012, 2095.

(8). Igarashi M; Watanabe T; Hashida T; Umekita M; Hatano M; Yanagida Y; Kino H; Kimura T; Kinoshita N; Inoue K; Sawa R; Nishimura Y; Utsumi R; Nomoto A J. Antibiot 2013, 66, 459–464.

(9). Elshahawi SI; Shaaban KA; Kharel MK; Thorson JS Chem. Soc. Rev 2015, 44, 7591–7697. [PubMed: 25735878]

(10). Martinez-Farina CF; Jakeman DL Chem. Commun. (Cambridge, U. K.) 2015, 51, 14617–14619.

(11). Forget SM; Martinez-Farina CF; Jakeman DL Chem. Commun. (Cambridge, U. K.) 2018, 54, 3544–3545.

(12). Lukoseviciute L; Lebedeva J; Kuisiene N Microb. Ecol 2021, 81, 110–121. [PubMed: 32638044]

(13). Ma M; Rateb ME; Teng Q; Yang D; Rudolf JD; Zhu X; Huang Y; Zhao LX; Jiang Y; Li X; Rader C; Duan Y; Shen B J. Nat. Prod 2015, 78, 2471–2480. [PubMed: 26335269]

(14). Kusumi S; Nakayama H; Kobayashi T; Kuriki H; Matsumoto Y; Takahashi D; Toshima K Chem. - Eur. J 2016, 22, 18733–18736. [PubMed: 27859867]

(15). Wu C; van der Heul HU; Melnik AV; Lubben J; Dorrestein PC; Minnaard AJ; Choi YH; van Wezel GP Angew. Chem., Int. Ed 2019, 58, 2809–2814.

(16). Mizia JC; Bennett CS Org. Lett 2019, 21, 5922–5927. [PubMed: 31305082]

(17). Kim GS; Kim GJ; Lee B; Oh TH; Kwon M; Lee JS; Jang JP; Choi H; Ko SK; Hong YS; Jang JH; Ahn JS J. Antibiot 2020, 73, 859–862.

(18). Voitsekhovskaia I; Paulus C; Dahlem C; Rebets Y; Nadmid S; Zapp J; Axenov-Gribanov D; Ruckert C; Timofeyev M; Kalinowski J; Kiemer AK; Luzhetskyy A Microorganisms 2020, 8, 680.

(19). Xu D; Nepal KK; Chen J; Harmody D; Zhu H; McCarthy PJ; Wright AE; Wang G Synth. Syst. Biotechnol 2018, 3, 246–251. [PubMed: 30417139]

(20). Acharya PP; Khatri HR; Janda S; Zhu J Org. Biomol. Chem 2019, 17, 2691–2704. [PubMed: 30768092]

(21). Qu XY; Ren JW; Peng AH; Lin SQ; Lu DD; Du QQ; Liu L; Li X; Li EW; Xie WD Mar. Drugs 2019, 17, 277.

(22). Ding WJ; Ji YY; Jiang YJ; Ying WJ; Fang ZY; Gao TT Biochem. Biophys. Res. Commun 2020, 531, 377–382. [PubMed: 32800334]

(23). Saito S; Kato W; Ikeda H; Katsuyama Y; Ohnishi Y; Imoto M J. Antibiot 2020, 73, 203–210.

(24). Yang L; Hou L; Li H; Li W Nat. Prod. Res 2020, 34, 3444–3450. [PubMed: 30835571]

(25). Wang W; Ji J; Li X; Wang J; Li S; Pan G; Fan K; Yang K Proc. Natl. Acad. Sci. U. S. A 2014, 111, 5688–5693. [PubMed: 24706927]

(26). Forget SM; Robertson AW; Overy DP; Kerr RG; Jakeman DL J. Nat. Prod 2017, 80, 1860–1866. [PubMed: 28520425]

(27). Huang C; Yang C; Zhang W; Zhang L; De BC; Zhu Y; Jiang X; Fang C; Zhang Q; Yuan CS; Liu HW; Zhang C Nat. Commun 2018, 9, 2088. [PubMed: 29802272]

(28). Kozasa T; Suzuki K; Tanaka K; Tsunoda N; Yoneda T; Ohata I Manufacture of anthraquinones as aldose reductase inhibitors by *streptomyces*. Patent Appl. JP 62093256 A, 1987.

(29). Wilton JH; Cheney DC; Hokanson GC; French JC; Cunheng H; Clardy J J. Org. Chem 1985, 50, 3936–3938.

(30). Kanamaru T; Nozaki Y; Muroi M TAN-1085 and its aglycon as angiogenesis and aromatase inhibitors and their manufacture with *Streptomyces species*. Patent Appl. JP 02289532 A, 1990.

(31). Hauser FM; Dorsch WA; Mal D Org. Lett 2002, 4, 2237–2239. [PubMed: 12074676]

(32). Wang X; Abbas M; Zhang Y; Elshahawi SI; Ponomareva LV; Cui Z; Van Lanen SG; Sajid I; Voss SR; Shaaban KA; Thorson JS J. Nat. Prod 2019, 82, 1686–1693. [PubMed: 31117525]

(33). Wang X; Zhang Y; Ponomareva LV; Qiu Q; Woodcock R; Elshahawi SI; Chen X; Zhou Z; Hatcher BE; Hower JC; Zhan C-G; Parkin S; Kharel MK; Voss SR; Shaaban KA; Thorson JS Angew. Chem., Int. Ed 2017, 56, 2994–2998.

(34). Zhang Y; Ye Q; Ponomareva LV; Cao Y; Liu Y; Cui Z; Van Lanen SG; Voss SR; She QB Chem. Sci 2019, 10, 7641–7648. [PubMed: 31583069]

(35). Ponomareva LV; Athippozhy A; Thorson JS; Voss SR Comp. Biochem. Physiol., Part C: Toxicol. Pharmacol 2015, 178, 128–135.

(36). Voss SR; Ponomareva LV; Dwaraka VB; Pardue KE; Baddar N; Rodgers AK; Woodcock MR; Qiu Q; Crowner A; Blichmann D; Khatri S; Thorson JS Sci. Rep 2019, 9, 6751. [PubMed: 31043677]

(37). Wang X; Elshahawi SI; Ponomareva LV; Ye Q; Liu Y; Copley GC; Hower JC; Hatcher BE; Kharel MK; Van Lanen SG; She QB; Voss SR; Thorson JS; Shaaban KA J. Nat. Prod 2019, 82, 3469–3476. [PubMed: 31833370]

(38). Cheema MT; Ponomareva LV; Liu T; Voss SR; Thorson JS; Shaaban KA; Sajid I Curr. Microbiol 2021. DOI: 10.1007/s00284-021-02557-y

(39). Fatima A; Aftab U; Shaaban KA; Thorson JS; Sajid I BMC Microbiol 2019, 19, 49. [PubMed: 30795744]

(40). Abbas M; Elshahawi SI; Wang X; Ponomareva LV; Sajid I; Shaaban KA; Thorson JS J. Nat. Prod 2018, 81, 2560–2566. [PubMed: 30418763]

(41). Laatsch H AntiBase 2017; Wiley-VCH: Weinheim, Germany, 2017.

(42). Matsuda H; Morikawa T; Toguchida I; Park JY; Harima S; Yoshikawa M Bioorg. Med. Chem 2001, 9, 41–50. [PubMed: 11197344]

(43). Chen WH; Chen J; Shi YP J. Asian Nat. Prod. Res 2011, 13, 1036–1041. [PubMed: 21985638]

(44). Igarashi Y; Yanase S; Sugimoto K; Enomoto M; Miyanaga S; Trujillo ME; Saiki I; Kuwahara SJ Nat. Prod 2011, 74, 862–865.

(45). Hu Y; Martinez ED; MacMillan JB J. Nat. Prod 2012, 75, 1759–1764. [PubMed: 23057874]

(46). Rohr J; Thiericke R Nat. Prod. Rep 1992, 9, 103–137. [PubMed: 1620493]

(47). Krohn K; Rohr J Top. Curr. Chem 1997, 188, 127–195.

(48). Zhu X; Siitonen V; Melançon CE Iii; Metsä-Ketelä M ACS Synth. Biol 2021, 10, 243–251. [PubMed: 33471506]

(49). Cao M; Zheng C; Yang D; Kalkreuter E; Adhikari A; Liu YC; Rateb ME; Shen B Angew. Chem., Int. Ed 2021, 60, 7140–7147.

(50). Kuntsmann MP; Mitscher LA J. Org. Chem 1966, 31, 2920–2925. [PubMed: 5919937]

(51). Rix U; Remsing LL; Hoffmeister D; Bechthold A; Rohr J ChemBioChem 2003, 4, 109–111. [PubMed: 12512084]

(52). Imamura N; Kakinuma K; Ikekawa N; Tanaka H; Omura SJ Antibiot 1982, 35, 602–608.

(53). Matsumoto T; Katsuki M; Jona H; Suzuki K J. Am. Chem. Soc 1991, 113, 6982–6992.

(54). Patrikainen P; Kallio P; Fan K; Klika KD; Shaaban KA; Mantsala P; Rohr J; Yang K; Niemi J; Metsä-Ketelä M Chem. Biol 2012, 19, 647–655. [PubMed: 22633416]

(55). Fan K; Zhang Q Synth. Syst. Biotechnol 2018, 3, 275–282. [PubMed: 30533539]

(56). Pan G; Gao X; Fan K; Liu J; Meng B; Gao J; Wang B; Zhang C; Han H; Ai G; Chen Y; Wu D; Liu ZJ; Yang K ACS Chem. Biol 2017, 12, 142–152. [PubMed: 28103689]

(57). Kricke P Ph.D. Thesis; University of Göttingen, 1984.

(58). Krohn K; Baltus W Tetrahedron 1988, 44, 49–54.

(59). Matsumoto T; Jona H; Katsuki M; Suzuki K Tetrahedron Lett 1991, 32, 5103–5106.

(60). Hong ST; Carney JR; Gould SJ J. Bacteriol 1997, 179, 470–476. [PubMed: 8990300]

(61). Chen Q; Mulzer M; Shi P; Beuning PJ; Coates GW; O'Doherty GA Org. Lett 2011, 13, 6592–6595. [PubMed: 22107019]

(62). Tawfike A; Attia EZ; Desoukey SY; Hajjar D; Makki AA; Schupp PJ; Edrada-Ebel R; Abdelmohsen UR AMB Express 2019, 9, 12. [PubMed: 30680548]

(63). Guo F; Xiang S; Li L; Wang B; Rajasarkka J; Grondahl-Yli-Hannuksela K; Ai G; Metsä-Ketelä M; Yang K Metab. Eng 2015, 28, 134–142. [PubMed: 25554073]

(64). Ye Q; Zhang Y; Cao Y; Wang X; Guo Y; Chen J; Horn J; Ponomareva LV; Chaiswing L; Shaaban KA; Wei Q; Anderson BD; St Clair DK; Zhu H; Leggas M; Thorson JS; She QB Cell. Chem. Biol 2019, 26, 366–377. [PubMed: 30661989]

(65). Dan VM; Vinodh JS; Sandesh CJ; Sanawar R; Lekshmi A; Kumar RA; Santhosh Kumar TR; Marelli UK; Dastager SG; Pillai MR ACS Chem. Biol 2020, 15, 780–788. [PubMed: 32058690]

(66). Panchuk RR; Lehka LV; Terenzi A; Matselyukh BP; Rohr J; Jha AK; Downey T; Kril IJ; Herbacek I; van Schoonhoven S; Heffeter P; Stoika RS; Berger W Free Radical Biol. Med 2017, 106, 134–147. [PubMed: 28189848]

(67). Lehka LV; Panchuk RR; Berger W; Rohr J; Stoika RS Ukr Biochem. J 2015, 87, 72–82. [PubMed: 26717598]

(68). Kharel MK; Pahari P; Shaaban KA; Wang G; Morris C; Rohr J Org. Biomol. Chem 2012, 10, 4256–4265. [PubMed: 22454092]

(69). Wang X; Shaaban KA; Elshahawi SI; Ponomareva LV; Sunkara M; Copley GC; Hower JC; Morris AJ; Kharel MK; Thorson JS J. Antibiot 2014, 67, 571–575.

(70). Shaaban KA; Wang X; Elshahawi SI; Ponomareva LV; Sunkara M; Copley GC; Hower JC; Morris AJ; Kharel MK; Thorson JS J. Nat. Prod 2013, 76, 1619–1626. [PubMed: 23947794]

(71). Wang X; Shaaban KA; Elshahawi SI; Ponomareva LV; Sunkara M; Zhang Y; Copley GC; Hower JC; Morris AJ; Kharel MK; Thorson JS J. Nat. Prod 2013, 76, 1441–1447. [PubMed: 23944931]

(72). Shaaban KA; Elshahawi SI; Wang X; Horn J; Kharel MK; Leggas M; Thorson JS J. Nat. Prod 2015, 78, 1723–1729. [PubMed: 26091285]

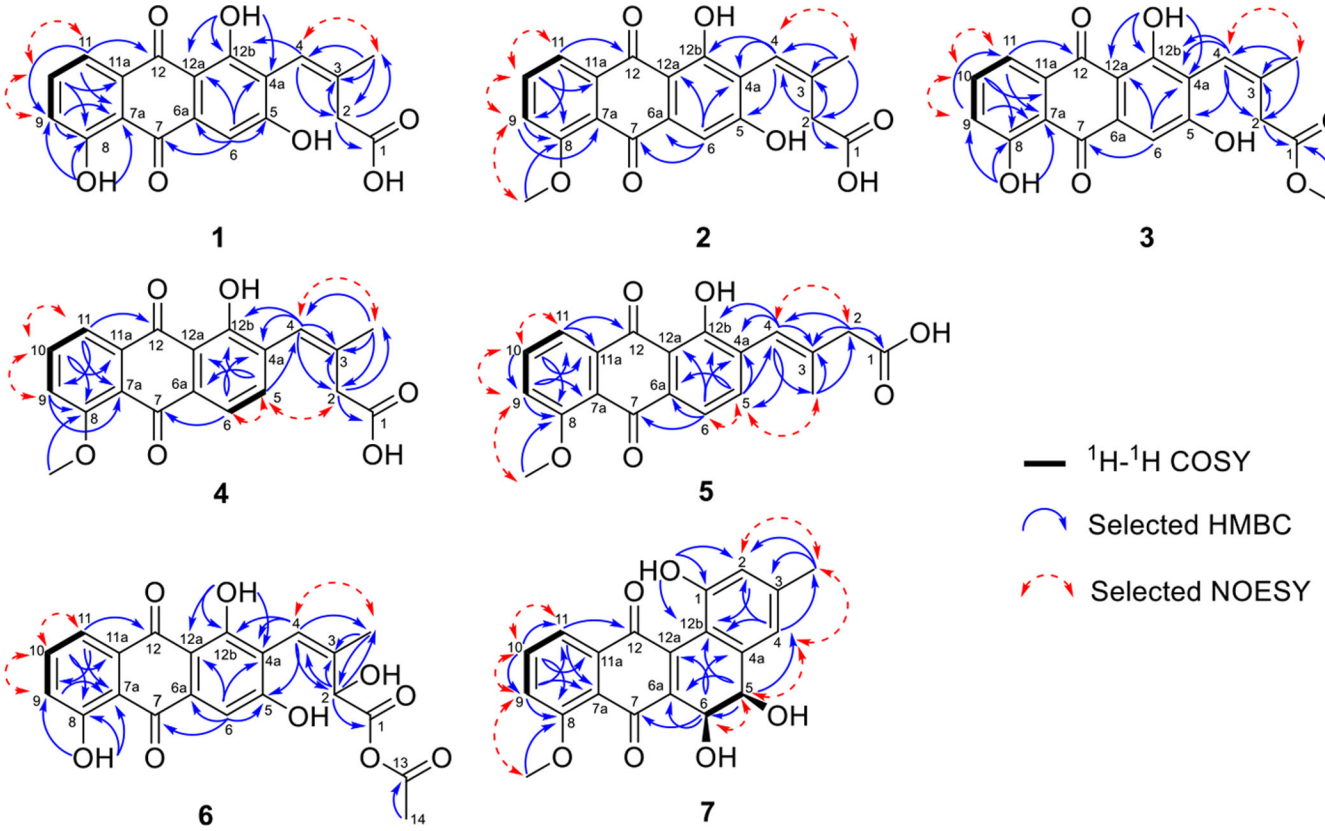

Figure 1.

^{1}H,^{1}H–COSY (——), selected HMBC (blue →) and selected NOESY (red ↔) correlations of himalaquinones A–G (**1**–**7**).

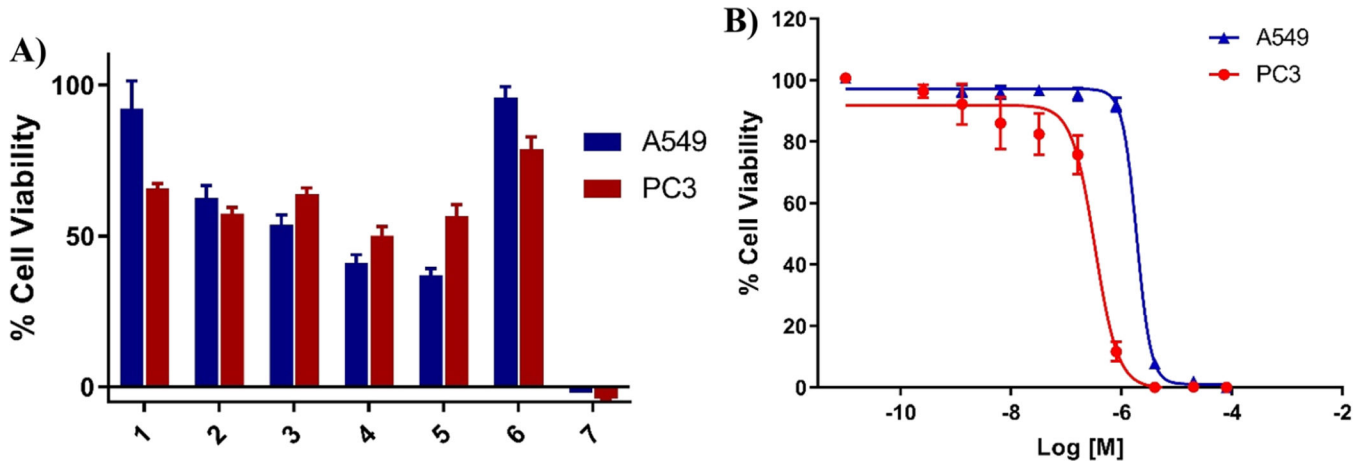

Figure 2.

(A) Percent viability of A549 (non-small-cell lung) and PC3 (prostate) human cancer cell lines (after 72 h) at 80 μM of compounds **1**–**7**. (B) Dose–response of compound **7** against A549 (non-small-cell lung) and PC3 (prostate) human cancer cell lines (72 h). See also Supporting Information, Figure S4 and Table S1.

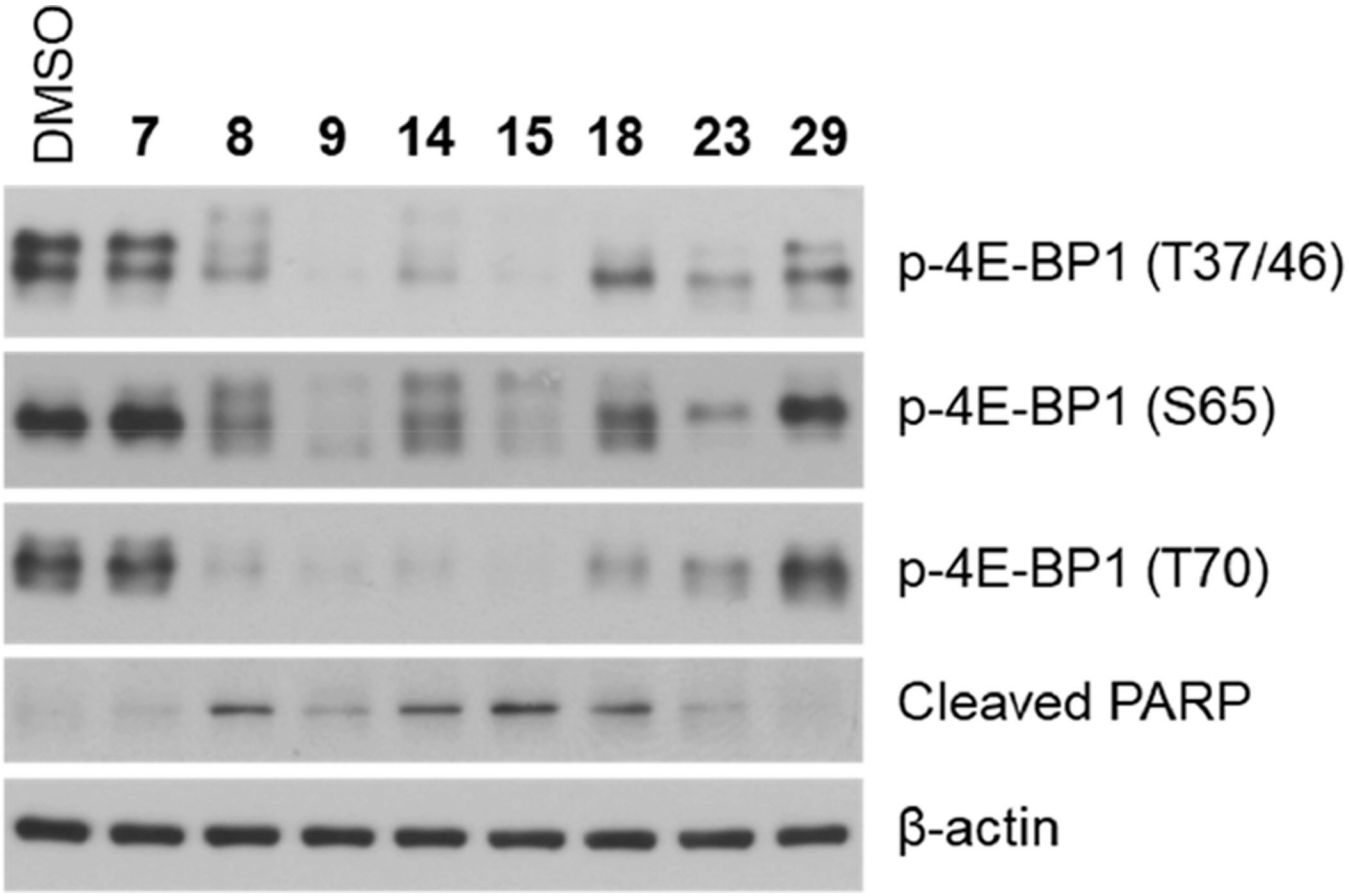

Figure 3.

HCT116 cells were treated with 2 μM of test compound [himalaquinone G (**7**), saquayamycins A (**8**), B (**9**), J (**14**), or K (**15**), or landomycins A (**18**), X (**23**), or Y (**29**)] or DMSO (negative control) for 6 h followed by Western blot analysis for the indicated proteins. The position of 4E-BP1 phosphorylation (p-4E-BP1) is indicated in parentheses, cleaved PARP is included as an apoptotic marker, and β-actin serves as an internal standard reference. For cancer cell line cytotoxicities (IC_{50}s), see Supporting Information, Table S1. For the chemical structures of compounds **1**–**31**, see Chart 1 and Figure 5.

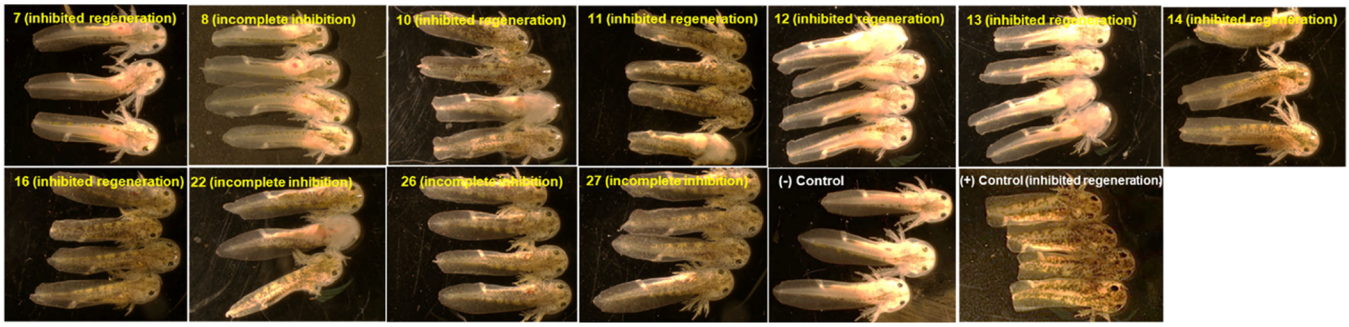

Figure 4.

Single-dose axolotl tail regeneration assay of himalaquinone G (**7**) and representative angucycline analogues saquayamycins A (**8**), B1 (**10**), G (**11**), H (**12**), I (**13**), and J (**14**), urdamycin A (**16**), and landomycins M (**26**), O (**27**), and V (**22**). All compounds were tested at 10 μM concentration with the exception of **8** (1.0 μM). Controls were 0.1% DMSO (negative) and Hsp90 inhibitor geldanamycin (positive). See Supporting Information, Table S1 for the summary results of compounds **1**–**31**. For the chemical structures of compounds **1**–**31**, see Chart 1 and Figure 5.

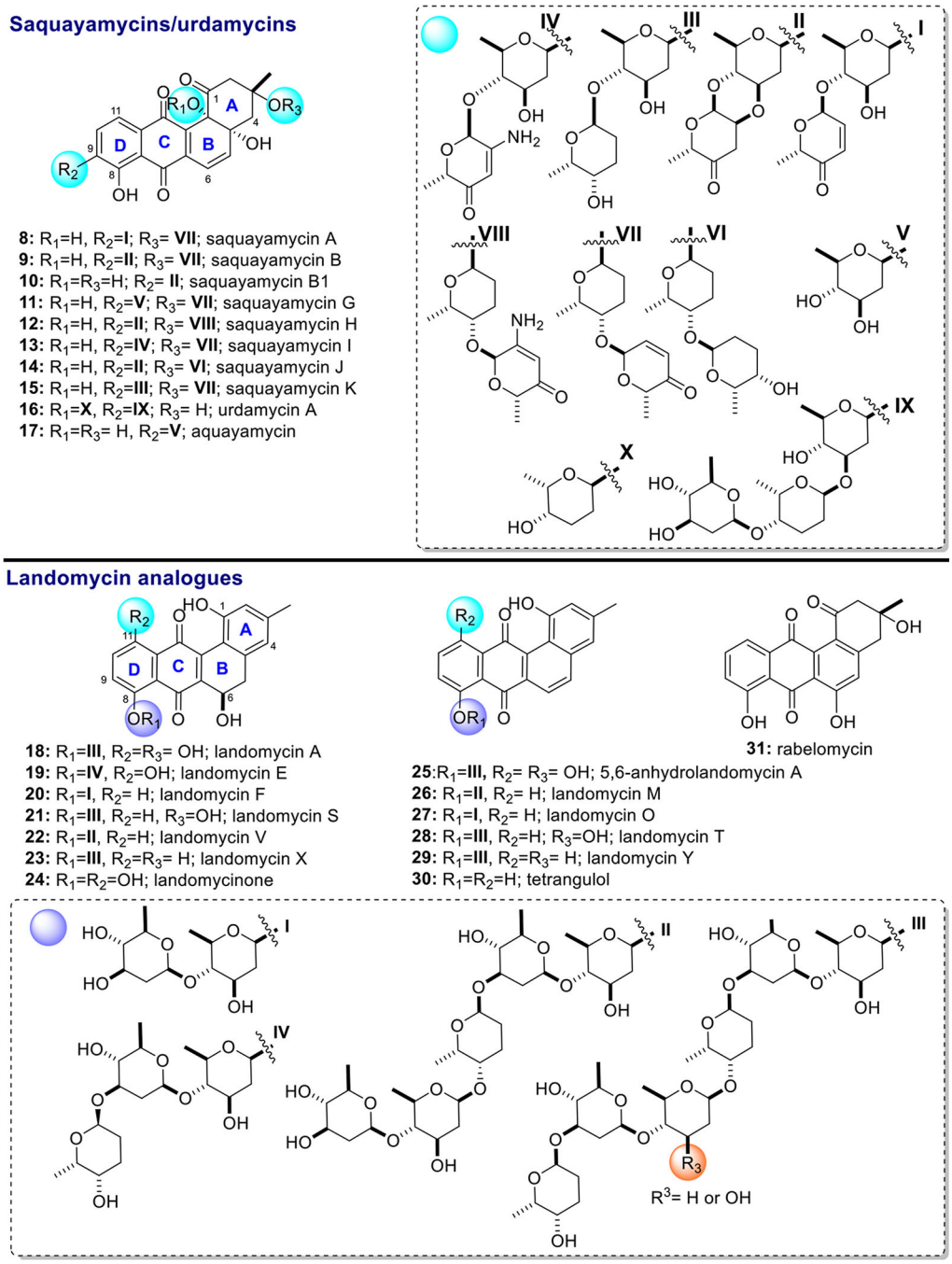

Figure 5.
Chemical structures of angucyclin(on)es **8**–**31**.

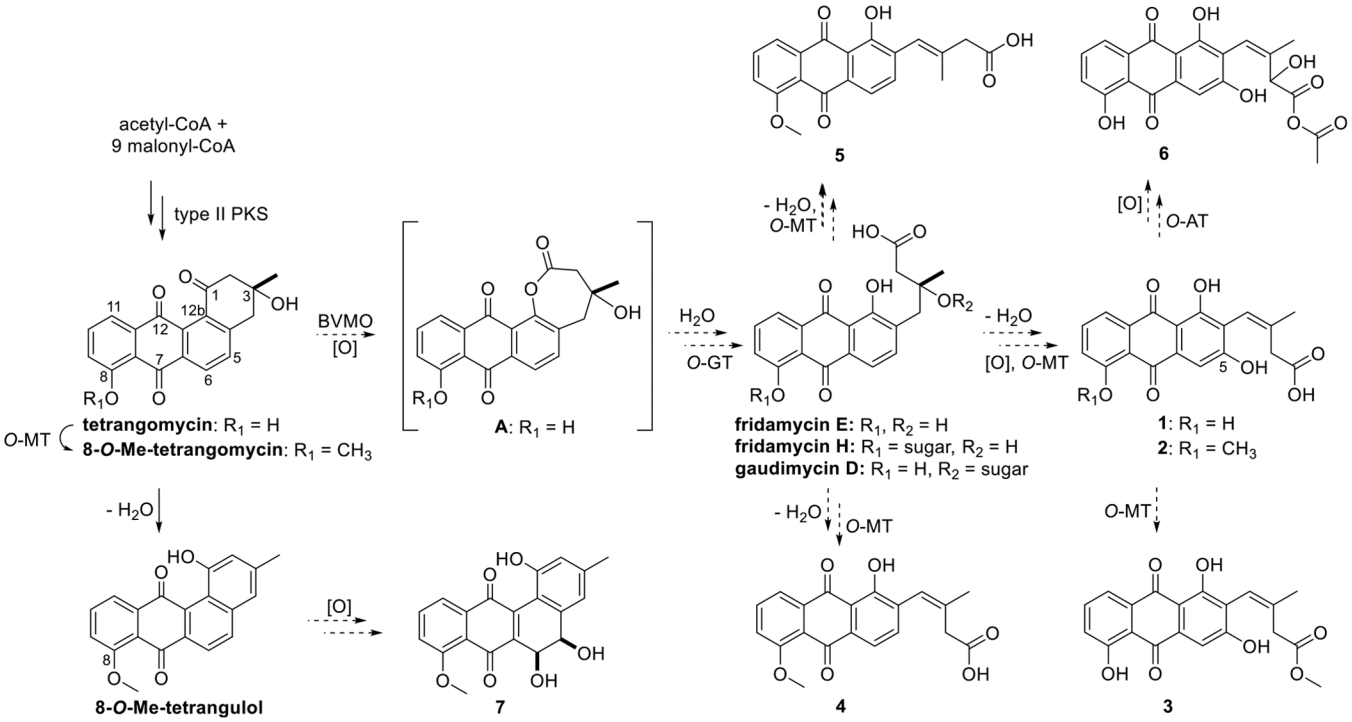

Scheme 1.

Proposed Biosynthetic Pathway of the Himalaquinones A–G (1–7)

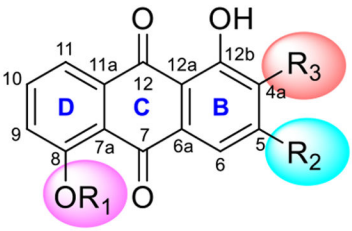

1: R_1=H, R_2=OH, R_3=**I**; Himalaquinone A
2: R_1=CH_3, R_2=OH, R_3=**I**; Himalaquinone B
3: R_1=H, R_2=OH, R_3=**II**; Himalaquinone C
4: R_1=CH_3, R_2=H, R_3=**I**; Himalaquinone D
5: R_1=CH_3, R_2=H, R_3=**III**; Himalaquinone E
6: R_1=H, R_2=OH, R_3=**IV**; Himalaquinone F

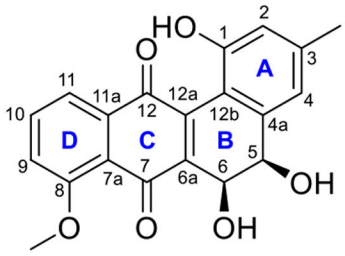

7: Himalaquinone G

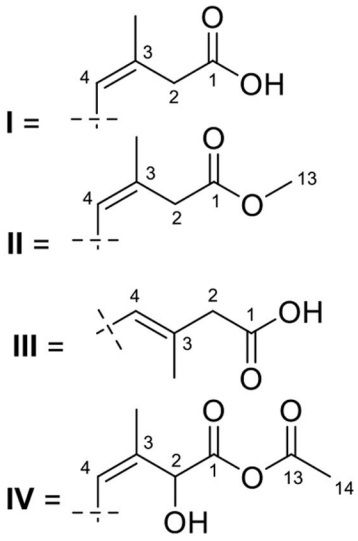

Chart 1.

Table 1.

^{13}C (100 MHz) NMR Spectroscopic Data for Compounds 1–7 in DMSO-d_6 (δ in ppm)[a]

	1	2	3	4	5	6	7
position	**δ_C, type**	**δ_C, type**	**δ_C, type**	**δ_C, type**	**δ_C, type**	**δ_C, type**	**δ_C, type**
1	172.0, C	172.0, C	170.9, C	172.1, C	172.2, C	169.4, C	155.4, C
2	39.6, CH_2	39.3, CH_2	39.1, CH_2	38.7, CH_2	45.3, CH_2	72.5, CH	117.0, CH
3	136.1, C	135.6, C	135.5, C	135.6, C	136.1, C	134.1, C	141.1, C
3-CH_3	23.9, CH_3	23.9, CH_3	23.9, CH_3	24.5, CH_3	18.4, CH_3	19.0, CH_3	21.0, CH_3
4	117.6, CH	117.5, CH	118.0, CH	121.8, CH	121.4, CH	121.6, CH	122.1, CH
4a	118.1, C	116.5, C	118.0, C	131.2, C	132.8, C	116.9, C	141.4, C
5	162.8, C	162.7, C	162.5, C	136.1, CH	136.7, CH	162.4, C	70.8, CH
6	108.2, CH	107.5, CH	107.8, CH	118.2, CH	118.1, CH	107.7, CH	62.6, CH
6a	132.2, C	134.4, C	132.5, C	133.0, C	131.3, C	132.8, C	139.8, C
7	187.2, C	180.3, C	187.2, C	180.2, C	180.2, C	187.1, C	181.9, C
7a	115.6, C	120.4, C	115.7, C	120.7, C	120.7, C	115.7, C	119.3, C
8	161.6, C	160.1, C	161.6, C	160.1, C	160.1, C	161.6, C	158.6, C
8-OCH_3		56.4, CH_3		56.5, CH_3	56.5, CH_3		56.3, CH_3
9	124.0, CH	119.2, CH	124.1, CH	119.9, CH	119.9, CH	124.1, CH	117.9, CH
10	137.2, CH	135.7, CH	137.3, CH	135.5, CH	135.5, CH	137.3, CH	134.8, CH
11	118.7, CH	118.7, CH	118.8, CH	118.9, CH	118.9, CH	118.8, CH	117.9, CH
11a	133.3, C	135.1, C	133.3, C	134.7, C	134.7, C	133.3, C	136.1, C
12	185.3, C	186.2, C	185.6, C	188.6, C	188.6, C	185.6, C	184.3, C
12a	108.7, C	108.5, C	109.0, C	115.0, C	114.9, C	108.9, C	140.2, C
12b	162.6, C	161.8, C	162.4, C	158.9, C	158.9, C	162.4, C	113.2, C
13			51.3, CH_3			169.7, C	
14						20.4, CH_3	

[a]See Supporting Information for NMR spectra. Assignments supported by 2D HSQC and HMBC experiments. Atom numbering based on angucyclinone structure **7**, for comparison.

Table 2.

^{1}H (400 MHz) NMR Spectroscopic Data for Compounds 1–7 in DMSO-d_6 (δ in ppm)[a]

	1	2	3	4	5	6	7
position	**δ_H (J in Hz)**	**δ_H (J in Hz)**	**δ_H (J in Hz)**	**δ_H (J in Hz)**	**δ_H (J in Hz)**	**δ_H (J in Hz)**	**δ_H (J in Hz)**
1-OH	11.80, br s	11.26, br s		12.50, br s	12.34, br s		9.64, s
2	2.90, s	2.89, s	2.98, s	3.12, s	3.22, s	5.43, d (0.9)	6.63, s
3-CH_3	1.99, d (0.9)	1.99, d (0.9)	1.99, d (1.2)	1.99, d (1.1)	1.89, s	1.91, s	2.26, s
4	6.00, s	6.01, s	6.06, d (1.0)	6.51, s	6.47, s	6.23, s	6.69, s
5				7.72, d (7.9)	7.72, d (8.0)		4.36, d (2.6)
5-OH	11.80, br s	11.97, br s	11.46, br s			11.55, br s	5.20, br s
6	7.24, s	7.19, s	7.31, s	7.61, overlap	7.61, overlap	7.32, s	4.87, d (2.5)
6-OH							5.20, br s
8-OH	12.38, s		12.40, s			12.36, s	
8-OCH_3		3.94, s		3.96, s	3.95, s		3.93, s
9	7.30, d (8.4)	7.59, d (8.6)	7.36, br dd (6.6, 0.9)	7.63, overlap	7.62, overlap	7.35, d (8.3)	7.51, overlap
10	7.75, t (8.0)	7.84, overlap	7.81, br dd (6.3, 6.7)	7.86, overlap	7.86, overlap	7.80, t (7.9)	7.77, t (8.0)
11	7.65, d (7.5)	7.85, overlap	7.73, br dd (6.1, 0.9)	7.87, overlap	7.86, overlap	7.72, d (7.5)	7.49, overlap
12b-OH	13.20, s	13.13, s	13.24, s	12.79, br s	12.82, br s	13.20, s	
13			3.56, s				
14						2.09, s	

[a]See Supporting Information for NMR spectra. Assignments supported by 2D HSQC and HMBC experiments. Atom numbering based on angucyclinone structure **7**, for comparison.